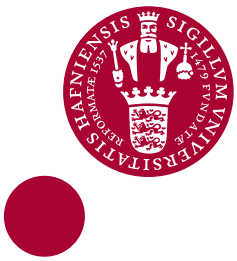

Unique developmental trajectories and genetic regulation of ventricular and outflow tract progenitors in the zebrafish second heart field

Paffett-Lugassy, Noelle; Novikov, Natasha; Jeffrey, Spencer; Abrial, Maryline; Guner-Ataman, Burcu; Sakthivel, Srinivasan; Burns, Caroline E.; Burns, C. Geoffrey

Published in:
Development (Cambridge)

DOI:
10.1242/dev.153411

Publication date:
2017

Document version
Publisher's PDF, also known as Version of record

© 2017. Published by The Company of Biologists Ltd | Development (2017) 144, 4616-4624 doi:10.1242/dev.153411

RESEARCH ARTICLE

Unique developmental trajectories and genetic regulation of ventricular and outflow tract progenitors in the zebrafish second heart field

Noelle Paffett-Lugassy[1,2,*], Natasha Novikov[1,2,*], Spencer Jeffrey[1], Maryline Abrial[1,2], Burcu Guner-Ataman[1,2], Srinivasan Sakthivel[1,3], Caroline E. Burns[1,2,4,‡] and C. Geoffrey Burns[1,2,‡]

ABSTRACT

During mammalian embryogenesis, cardiac progenitor cells constituting the second heart field (SHF) give rise to the right ventricle and primitive outflow tract (OFT). In zebrafish, previous lineage-tracing and mutant analyses suggested that SHF ventricular and OFT progenitors co-migrate to the arterial pole of the zebrafish heart tube soon after their specification in the *nkx2.5*$^+$ field of anterior lateral plate mesoderm (ALPM). Using additional prospective lineage tracing, we demonstrate that while SHF ventricular progenitors migrate directly to the arterial pole, OFT progenitors become temporarily sequestered in the mesodermal cores of pharyngeal arch 2 (PA2), where they downregulate *nkx2.5* expression. While there, they intermingle with precursors for PA2-derived head muscles (HMs) and hypobranchial artery endothelium, which we demonstrate are co-specified with SHF progenitors in the *nkx2.5*$^+$ ALPM. Soon after their sequestration in PA2, OFT progenitors migrate to the arterial pole of the heart and differentiate into OFT lineages. Lastly, we demonstrate that SHF ventricular and OFT progenitors exhibit unique sensitivities to a mutation in *fgf8a*. Our data highlight novel aspects of SHF, OFT and HM development in zebrafish that will inform mechanistic interpretations of cardiopharyngeal phenotypes in zebrafish models of human congenital disorders.

KEY WORDS: Zebrafish, Cardiac progenitors, Second heart field, Outflow tract, Congenital heart disease, *nkx2.5*

INTRODUCTION

During mammalian embryogenesis, cardiac progenitor cells in the anterior second heart field (SHF) produce the right ventricle and embryonic outflow tract (OFT) through late differentiation and accretion from pharyngeal mesoderm to the arterial pole of the heart tube (reviewed by Abu-Issa and Kirby, 2007; Vincent and Buckingham, 2010; Zaffran and Kelly, 2012). Before localizing to pharyngeal mesoderm, SHF progenitors are specified in lateral plate mesoderm when they initiate expression of several cardiac transcription factors, including *nkx2.5* (Stanley et al., 2002; Zhang et al., 2014).

As conduits for blood exiting the heart, OFTs share common structural features across vertebrate species. Specifically, they comprise proximal (relative to blood flow) myocardial segments, middle segments with overlapping myocardium and smooth muscle, and distal segments composed exclusively of smooth muscle, all of which encase lumenal endocardium (Grimes et al., 2010). In higher vertebrates, the embryonic OFT is a relatively long transient structure with extensive myocardium (Waldo et al., 2005), which becomes intricately remodeled through wall rotation (Bajolle et al., 2006), tubular compaction (Watanabe et al., 1998), septation (Kirby, 2007) and aortic wedging (Kirby, 2007). These morphogenetic events serve to create an exclusive connection between each great artery and the appropriate ventricle. Defects in OFT morphogenesis or remodeling cause a class of common congenital heart defects (Benjamin et al., 2017) (i.e. conotruncal malformations) characterized by misalignment of the great arteries with the ventricles or a common arterial trunk, respectively (Kirby, 2007). In both cases, deoxygenated blood mixes with oxygenated blood, which necessitates surgical repair of the malformation. Therefore, deciphering the molecular and cellular determinants of OFT morphogenesis remains an important area of investigation for preventing and managing congenital heart defects.

Zebrafish hearts contain a single ventricle and OFT composed of a relatively short myocardial base and taller elastin2$^+$ (Eln2$^+$) smooth muscle collar known as the bulbus arteriosus, both of which surround OFT endocardium (Grimes et al., 2006; Miao et al., 2007). Unlike in higher vertebrates, the zebrafish OFT does not become remodeled or septated. Recent studies have demonstrated that half of the ventricular myocardium and three OFT lineages in zebrafish derive from cardiac progenitors with defining features of the anterior SHF (de Pater et al., 2009; Guner-Ataman et al., 2013; Hami et al., 2011; Lazic and Scott, 2011; Zhou et al., 2011). Specifically, SHF progenitors for the distal ventricular myocardium are specified bilaterally in *nkx2.5*$^+$ anterior lateral plate mesoderm (ALPM) before migrating to the arterial pole of the linear heart tube, where they undergo late myocardial differentiation and accretion to the heart. Evidence for myocardial accretion was uncovered when dye-labeled pharyngeal mesodermal cells were subsequently localized to the distal ventricle (Hami et al., 2011; Zhou et al., 2011).

Based on genetic lineage-tracing and mutant analyses, it was assumed that SHF progenitors for the OFT, also specified as *nkx2.5*$^+$ cells in the ALPM (Guner-Ataman et al., 2013; Hami et al., 2011), were either one and the same with SHF ventricular progenitors or followed the same trajectory to the arterial pole of the linear heart tube. This assumption was based on co-labeling of the distal ventricle and OFT in the lineage trace of *ltbp3*$^+$ SHF cells and the observation

[1]Cardiovascular Research Center, Massachusetts General Hospital, Charlestown, MA 02129, USA. [2]Harvard Medical School, Boston, MA 02115, USA. [3]Department of Cellular and Molecular Medicine, Faculty of Health and Medical Sciences, University of Copenhagen, Copenhagen DK-2200N, Denmark. [4]Harvard Stem Cell Institute, Cambridge, MA 02138, USA.
*These authors contributed equally to this work

‡Authors for correspondence (cburns6@mgh.harvard.edu; gburns@cvrc.mgh.harvard.edu)

N.P., 0000-0003-1441-651X; C.G.B., 0000-0002-5812-6621

Received 20 April 2017; Accepted 11 October 2017

Development (2017) 144, 4616-4624 doi:10.1242/dev.153411

that *ltbp3* expression initiates in SHF progenitors as they reach the midline (Zhou et al., 2011). Moreover, four loss-of-function experimental groups – *ltbp3* morphants (Zhou et al., 2011), *mef2cab* morphants (Lazic and Scott, 2011), *smoothened* null animals (Hami et al., 2011) and *tbx1* mutants (Hami et al., 2011; Nevis et al., 2013) – exhibited reductions or deficiencies in both SHF-derived ventricular and OFT lineages. These findings suggested that a single progenitor population, compromised in these animals, might be giving rise to both the distal ventricle and OFT. In this scenario, after SHF progenitors complete myocardial accretion to the ventricle, the same progenitor population would produce OFT lineages. Despite the plausibility of this hypothesis, evidence to support or refute this notion has yet to be provided.

Here, we report that, contrary to the previous assumption, SHF ventricular and OFT progenitors take unique trajectories to the arterial pole of the heart. Whereas SHF ventricular precursors migrate directly to the midline and maintain *nkx2.5* expression, OFT progenitors remain lateral and become temporarily sequestered in pharyngeal arch (PA) 2, where they downregulate *nkx2.5*. While there, OFT progenitors are in close apposition to precursors for PA2-derived head muscles (HMs) and hypobranchial artery (HA) endothelium, both of which are co-specified in the *nkx2.5*$^{+}$ ALPM. Last, whereas mutations in *fgf8a* compromise SHF ventricular development, the OFT and PA2-derived head muscles are unaffected, demonstrating that progenitor compartmentalization in PA2 confers unique genetic regulatory mechanisms to this population. Taken together, our data illuminate previously unappreciated aspects of SHF, OFT and HM development in zebrafish that will become instrumental for guiding future studies designed to understand the cellular mechanisms of cardiopharyngeal phenotypes in zebrafish models of human congenital craniofacial and cardiovascular malformations.

RESULTS

Zebrafish *nkx2.5 cis*-regulatory elements label a subset of head muscles and hypobranchial artery endothelium in *nkx2.5:ZsYellow* transgenic embryos

We have reported previously that transgenic zebrafish embryos expressing ZsYellow from *nkx2.5 cis*-regulatory sequences display reporter fluorescence in the atrium, ventricle, OFT, ventral aorta and pharyngeal arch arteries (PAAs) by 60 hours post-fertilization (hpf) (Nevis et al., 2013; Paffett-Lugassy et al., 2013). Upon closer examination of 72 hpf *Tg(nkx2.5:ZsYellow)* larvae, immunostained for ZsYellow, we observed the reporter in a subset of HMs, including the ventral and middle PA1 (mandibular) muscles, as well as all five PA2 (hyoid) muscles (Fig. 1A-F) (Schilling and Kimmel, 1997). Additionally, ZsYellow was colocalized with endothelial cells composing the HAs (Fig. 1G-I). Last, ZsYellow was observed in the outermost layer of the pericardial sac (Fig. 1A-C). These data are consistent with, and provide higher resolution for, a previous description of ZsYellow expression in *Tg(nkx2.5:ZsYellow)* animals (Nagelberg et al., 2015).

To determine whether the presence of ZsYellow in HMs, HA endothelium and the heart mirrored ongoing *nkx2.5* expression, we localized endogenous transcripts in 72 hpf wild-type animals by *in situ* hybridization. Although *nkx2.5* transcripts were abundant in the cardiac chambers, they were absent from the HMs, HA endothelium and the smooth muscle collar of the OFT and underlying endocardium (Fig. S1A). The same structures were also devoid of ZsYellow transcripts in *Tg(nkx2.5:ZsYellow)* larvae (Fig. S1B-F), suggesting that their ZsYellow positivity (Fig. 1A-I, Fig. S1D-F) stems from residual protein produced earlier in development by progenitor cells for these lineages.

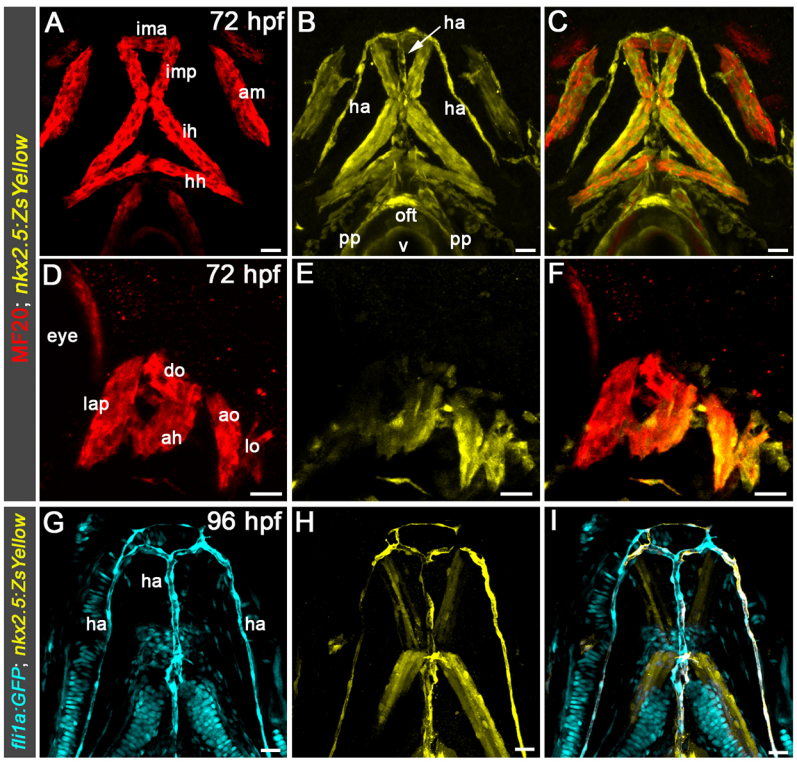

Fig. 1. Identification of ZsYellow^{+} head muscles and endothelium in *Tg(nkx2.5:ZsYellow)* larvae. (A-F) Confocal *z*-stacks of pharyngeal regions in 72 hpf *Tg(nkx2.5:ZsYellow)* zebrafish larvae double immunostained to detect ZsYellow fluorescent protein and striated muscle (MF20 antibody) imaged in the green (pseudocolored yellow) and red channels, respectively. (G-I) Confocal *z*-stacks of the pharyngeal region in a 96 hpf *Tg(nkx2.5:ZsYellow)*; *Tg(fli1a:GFP)* larvae double immunostained to detect ZsYellow and green fluorescent protein (GFP) imaged in the red (pseudocolored yellow) and green (pseudocolored cyan) channels, respectively. Single-channel (A,B,D,E,G,H) and merged (C,F,I) images are shown. Ventral (A-C,G-I) and lateral (D-F) views are shown. Anterior is upwards (A-C,G-I) or leftwards (D-F). For both experiments, little to no variability in the staining patterns was observed in the greater than 30 animals examined. Ventral pharyngeal arch (PA) 1 (mandibular) muscle: ima, intermandibular anterior. Middle PA1 muscles: imp, intermandibular posterior; am, adductor mandibulae. Dorsal PA1 muscles: lap, levator arcus palatine; do, dilator operculi. Ventral PA2 (hyoid) muscle: ih, interhyal. Middle PA2 muscle: hh, hyohyal. Dorsal PA2 muscles: ah, adductor hyomandibulae; ao, adductor operculi; lo, levator operculi. Vessel: ha, hypobranchial artery. Cardiac structures: oft, outflow tract; pp, parietal pericardium; v, ventricle. Scale bars: 25 µm.

Development (2017) 144, 4616-4624 doi:10.1242/dev.153411

Visualization of head muscle and endothelial progenitors in the anterior pharyngeal arches

We sought to visualize and lineage trace HM and HA endothelial progenitor cells at progressively earlier developmental stages to identify when and where they express *nkx2.5*. A previous study reported that myoblasts for PA1 and PA2 muscles initiate MyoD^{+} expression within the mesodermal cores of their respective PAs by 55 hpf (Schilling and Kimmel, 1997). The arches themselves arise through anterior-to-posterior segmentation of the pharynx, a process that is largely complete by 30 hpf (Schilling and Kimmel, 1994). Therefore, we examined PA1 and PA2 in *Tg(nkx2.5:ZsYellow)* animals at two stages prior to the initiation of MyoD expression but after pharyngeal segmentation in an attempt to visualize ZsYellow^{+} myoblast precursors. To unequivocally identify the mesodermal cores of the arches, we used a second transgene, *Tg(fli1a:GFP)*, that drives GFP expression in cranial neural crest-derived cells surrounding the cores (Lawson and Weinstein, 2002).

At a developmental stage corresponding to the end of pharyngeal segmentation (28 hpf), ZsYellow^{+} cells were observed in PA1 and PA2 surrounded by, but not overlapping with, GFP fluorescence (Fig. 2A-D, Fig. S2A-C), indicative of mesodermal core localization. At 48 hpf, clusters of ZsYellow^{+} cells, also non-overlapping with surrounding GFP fluorescence, were located ventrally in both arches and dorsally in PA2 (Fig. 2E-H, Fig. S2D-F), all of which represent locations where myoblasts initiate MyoD expression by 55 hpf (Schilling and Kimmel, 1997). Notably absent was a cluster of ZsYellow^{+} cells in a dorsal location within PA1 (Fig. S2D-I) where progenitors reside for the two dorsal PA1 muscles, which are negative for ZsYellow in *Tg(nkx2.5:ZsYellow)* animals (Fig. 1D-F). Last, we corroborated that ZsYellow^{+} cells reside in the mesodermal cores of PA2 using the *Tg(sox10:GFP)* reporter for neural crest-derived cells (Carney et al., 2006) (Fig. S2J-L).

To determine whether ZsYellow reporter fluorescence in PA1 and PA2 (Fig. 2A-H, Fig. S2A-F) reflected ongoing *nkx2.5* expression, we performed *in situ* hybridization for endogenous transcripts in wild-type embryos at the same developmental stages. At 28 hpf, we detected *nkx2.5* expression in PA2 (Fig. S1G). We reported previously that *nkx2.5* expression becomes undetectable in the pharynx by 48 hpf (Paffett-Lugassy et al., 2013), which demonstrates that *nkx2.5* messages disappear from PA2 between 28 hpf and 48 hpf. We did not detect *nkx2.5* expression in PA1 at 28 hpf (Fig. S1G). Based on lineage-tracing experiments detailed below, we predict that *nkx2.5* expression occurs transiently in PA1

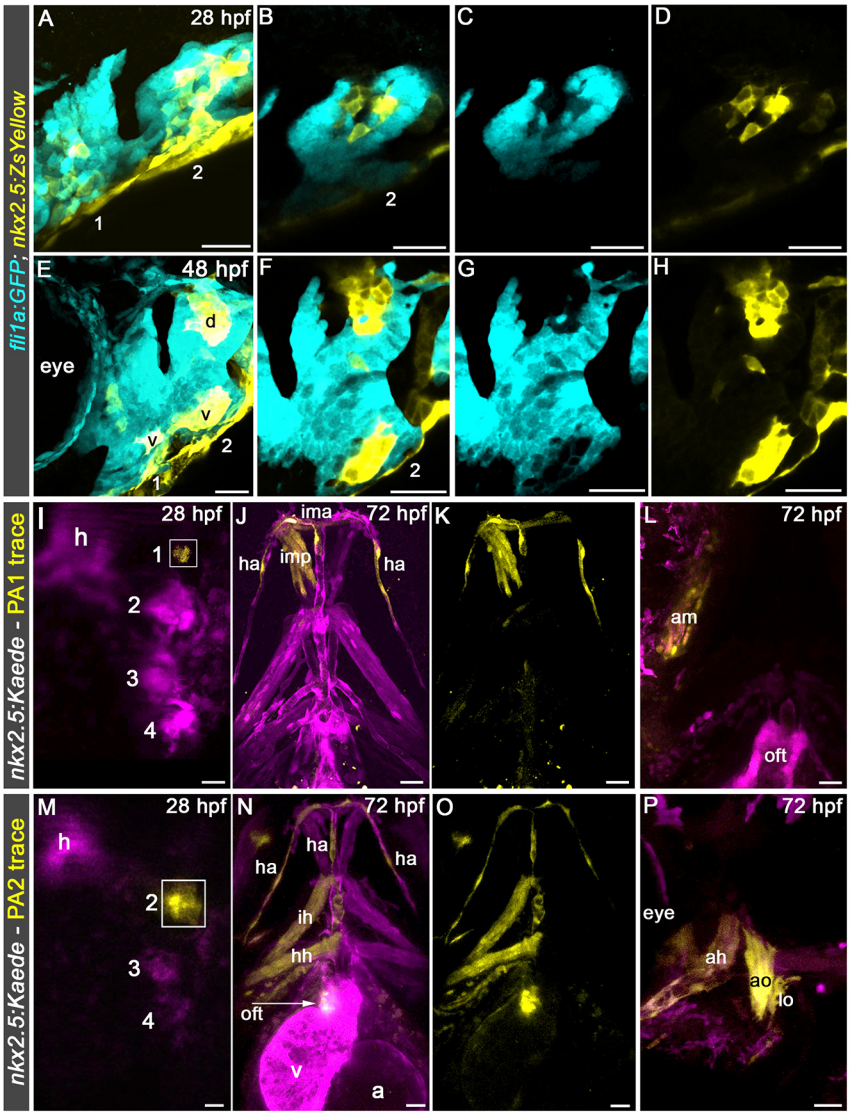

Fig. 2. Visualization and prospective lineage tracing of head muscle and hypobranchial artery endothelial precursors in pharyngeal arches 1 and 2. (A-H) Confocal images of pharyngeal arch (PA) 1 and PA2 in 28 hpf (A-D) and 48 hpf (E-H) *Tg(nkx2.5:ZsYellow); Tg(fli1a:GFP)* embryos double immunostained for GFP and ZsYellow imaged in the green (pseudocolored cyan) and red (pseudocolored yellow) channels, respectively. Single planes (B-D,F-H) from merged confocal *z*-stacks (A,E) are shown as merged (B,F) or single-channel (C,D,G,H) images. Left lateral views are shown. Anterior is towards the left. Little to no variability was observed in greater than 30 animals examined. (I,M) Merged confocal *z*-stacks of pharyngeal regions in live 28 hpf *Tg(nkx2.5:Kaede)* embryos immediately following unilateral photoconversion of Kaede^{+} cells (boxed regions) in PA1 (I) or PA2 (M). (J,K,N,O) Confocal *z*-stacks of pharyngeal regions in the same embryos at 72 hpf shown as merged (J,L,N,P) or single-channel (K,O) images. All five animals with PA1 photoconversion demonstrated tracing to the ipsilateral PA1 head muscles and bilateral HA endothelium. Labeling of the intermandibular anterior muscle crossed the midline in some cases. All 14 animals with PA2 photoconversion demonstrated tracing to the ipsilateral PA2 head muscles, ipsilateral OFT and bilateral HA endothelium. Animals were imaged in the green (pseudocolored magenta) and red (pseudocolored yellow) channels. Dorsal (I,M), ventral (J,K,N,O) and lateral (L,P) views are shown. Anterior is upwards (I-K,M-O) or leftwards (L,P). Numbers label the pharyngeal arches. d, dorsal cluster; v, ventral cluster. Ventral pharyngeal arch (PA) 1 (mandibular) muscle: ima, intermandibular anterior. Middle PA1 muscles: imp, intermandibular posterior; am, adductor mandibulae. Ventral PA2 (hyoid) muscle: ih, interhyal. Middle PA2 muscle: hh, hyohyal. Dorsal PA2 muscles: ah, adductor hyomandibulae; ao, adductor operculi; lo, levator operculi. Vessel: ha, hypobranchial artery. Cardiac structures: oft, outflow tract; a, atrium; v, ventricle. Scale bars: 25 µm.

Development (2017) 144, 4616-4624 doi:10.1242/dev.153411

between the 14-somite stage (ss; 16 hpf) and 28 hpf. Consistent with this conclusion, we detected *ZsYellow* transcripts in PA1 of *Tg(nkx2.5:ZsYellow)* animals at 28 hpf (Fig. S1H), likely because *ZsYellow* mRNAs produced transiently in PA1 from *nkx2.5 cis*-regulatory elements persist longer than endogenous *nkx2.5* transcripts.

Lineage tracing head muscle and endothelial precursors in pharyngeal arches 1 and 2

Next, we prospectively lineage traced the presumptive ZsYellow^{+} myoblast precursors in PA1 and PA2 to uncover their fates. To achieve this, we used a previously validated transgenic strain, *Tg(nkx2.5:Kaede)* (Guner-Ataman et al., 2013; Paffett-Lugassy et al., 2013), that expresses the photoconvertible Kaede protein from *nkx2.5 cis*-regulatory elements. A confocal laser scanning microscope was used to achieve targeted photoconversion of Kaede^{+} cells in PA1 or PA2 at 28 hpf. The same animals were evaluated at 72 hpf for labeling of HMs with the photoconverted Kaede protein (Kaede^{PC}). Following unilateral photoconversion of Kaede^{+} cells in PA1 (Fig. 2I), we observed Kaede^{PC} signals in the ventral and middle PA1 muscles on the same side of the embryo (Fig. 2J-L). Unilateral photoconversion of Kaede^{+} cells in PA2 (Fig. 2M) caused all five PA2 muscles on the same side of the embryo to become positive for Kaede^{PC} (Fig. 2N-P). These data demonstrate that *nkx2.5 cis*-regulatory elements label myoblast precursors for all PA1 and PA2 muscles, except the two dorsal PA1 muscles. Moreover, to our knowledge, this study represents the first prospective lineage tracing of myoblast precursors localized in the anterior PAs.

Unilateral photoconversion of Kaede^{+} cells in PA1 or PA2 (Fig. 2I,M) also caused Kaede^{PC} labeling of HA endothelium (Fig. 2J,K,N,O), indicating that HM and endothelial progenitors are one and the same or closely apposed in the PAs. Interestingly, although myoblast precursors give rise to muscles exclusively on the same side of the embryo, HA endothelial precursors cross the midline because unilateral photoconversion of Kaede^{+} cells resulted in bilateral Kaede^{PC} labeling of HA endothelium (Fig. 2J,K,N,O). Unexpectedly, photoconverting Kaede^{+} cells in PA2 caused cells within the OFT on the photoconverted side to become labeled with Kaede^{PC} (Fig. 2M-O; see below), suggesting that SHF OFT progenitors are also among HM and HA endothelial precursors in PA2.

Lineage tracing *nkx2.5*$^{+}$ head muscle and endothelial precursors in PA2 from the ALPM

nkx2.5 transcripts become detectable initially in zebrafish embryos by 6 ss (12 hpf) (Lee et al., 1996; Schoenebeck et al., 2007) in a bilateral population of ALPM cells comprising progenitors for ventricular myocardium (Guner-Ataman et al., 2013; Hami et al., 2011; Schoenebeck et al., 2007; Serbedzija et al., 1998), OFT lineages (Guner-Ataman et al., 2013; Hami et al., 2011) and endothelial cells that make up the VA and PAAs (Paffett-Lugassy et al., 2013). We hypothesized that the HM, HA endothelial and OFT progenitors residing in PA1 and/or PA2 (Fig. 2I,M) initiate *nkx2.5* expression in the ALPM.

To test this hypothesis, we unilaterally photoconverted Kaede^{+} cells in the anterior half of the ALPM in 14 ss (16 hpf) *Tg(nkx2.5:Kaede)* embryos (Fig. 3A-C) and analyzed the same embryos at 28 hpf for Kaede^{PC} expression in PA1 and PA2. As anticipated, we detected Kaede^{PC} fluorescence in the ventricular segment of the heart tube and in SHF progenitors at its arterial pole (Fig. 3D-F) (Zhou et al., 2011). We also observed Kaede^{PC+} cells in PA2 (Fig. 3D-F), demonstrating that these progenitors are specified in the ALPM. PA1, although negative for Kaede^{PC+} cells, harbored a cluster of cells expressing the native Kaede protein (Fig. 3D-F), indicating that they initiated Kaede expression after 14 ss.

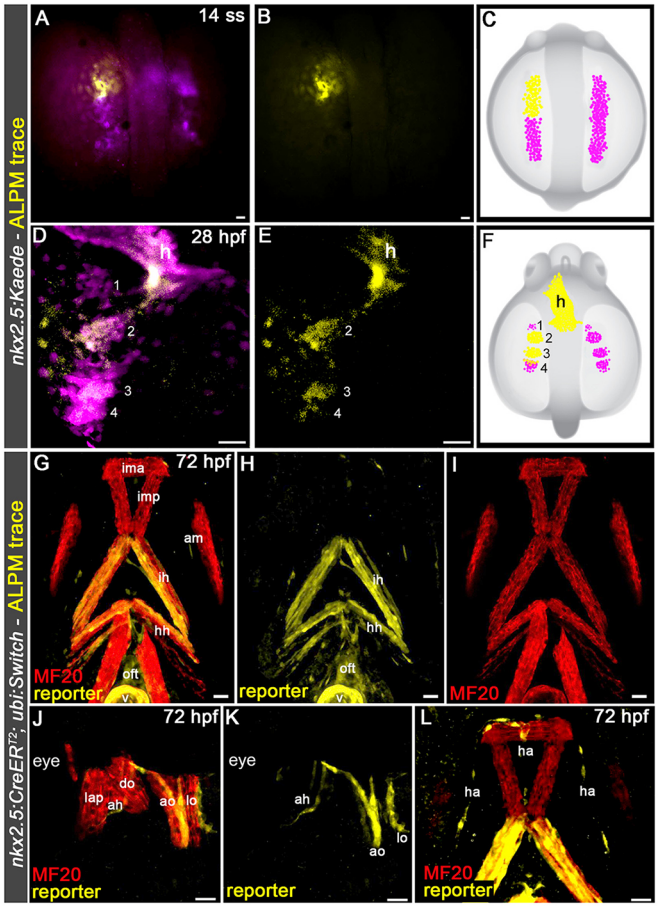

Fig. 3. Pharyngeal arch 2 muscles and hypobranchial artery endothelium derive from *nkx2.5*$^{+}$ progenitors in the ALPM. (A-F) Confocal *z*-stacks (A,B, D,E) and schematic diagrams (C,F) of a 14-somite stage (ss) (16 hpf) *Tg(nkx2.5:Kaede)* embryo immediately following left-side photoconversion of the Kaede^{+} ALPM (anterior half; A-C) and the same embryo at 28 hpf (D-F) imaged in the green (pseudocolored magenta) and red (pseudocolored yellow) channels. Dorsal views are shown. Anterior is upwards. Merged (A,D) and single-channel (B,E) images are shown. In all five embryos, photoconverted cells traced to the heart and the pharyngeal arches as shown. (G-L) Confocal *z*-stacks of pharyngeal regions in 72 hpf *Tg(nkx2.5:CreER^{T2}), Tg(ubi:Switch)* embryos pulsed with 4-OHT between tailbud and 16 ss (10-17 hpf). Animals were double immunostained to detect the mCherry reporter protein and striated muscle (MF20 antibody) before imaging in the red (pseudocolored yellow) and far-red (pseudocolored red) channels, respectively. Ventral (G-I,L) and left lateral (J,K) views are shown. Anterior is upwards (G-I,L) or leftwards (J,K). All 12 animals exhibited lineage tracing to the described structures. Numbers label the pharyngeal arches. h, heart. Ventral pharyngeal arch (PA) 1 (mandibular) muscle: ima, intermandibular anterior. Middle PA1 muscles: imp, intermandibular posterior; am, adductor mandibulae. Dorsal PA1 muscles: lap, levator arcus palatine; do, dilator operculi. Ventral PA2 (hyoid) muscle: ih, interhyal. Middle PA2 muscle: hh, hyohyal. Dorsal PA2 muscles: ah, adductor hyomandibulae; ao, adductor operculi; lo, levator operculi. Vessel: ha, hypobranchial artery. Cardiac structures: oft, outflow tract; v, ventricle. Scale bars: 25 µm.

Next, we used a complementary experimental approach to test the hypothesis that HM and endothelial progenitors in PA2, but not PA1, derive from *nkx2.5*$^{+}$ cells in the ALPM. We employed a previously characterized two-part transgenic system for prospective lineage tracing of *nkx2.5*$^{+}$ cells (Guner-Ataman et al., 2013;

Development (2017) 144, 4616-4624 doi:10.1242/dev.153411

Paffett-Lugassy et al., 2013). The system comprises a *Tg(nkx2.5:CreER^{T2})* driver transgene, to achieve 4-OHT-induced activation of Cre recombinase, and a ubiquitous reporter transgene termed *ubi:Switch* (Mosimann et al., 2011). In double transgenic embryos, we activated Cre transiently between tail bud and 12-16 ss (10 to 15-17 hpf), a developmental window that overlaps with the initiation of *nkx2.5* expression in the ALPM (Lee et al., 1996; Schoenebeck et al., 2007), and analyzed embryos for reporter expression at 72 hpf. As documented previously, we observed reporter fluorescence in the ventricle, OFT and PAAs (Fig. 3G-I and data not shown) (Guner-Ataman et al., 2013; Paffett-Lugassy et al., 2013). Furthermore, in these animals, all five PA2 muscles (Fig. 3G-K) and HA endothelium (Fig. 3L) were labeled, demonstrating that HM and HA endothelial cells are newly appreciated fates of *nkx2.5*$^{+}$ cells in the ALPM. We never observed PA1 muscles labeled when 4-OHT exposure ceased at 12 ss. When 4-OHT was removed at 16 ss, a minority of animals showed labeling in PA1 muscles (data not shown), which provides further evidence that PA1 muscle progenitors are specified subsequent to those for PA2.

Finally, we monitored the behavior of ZsYellow^{+} cells in the ALPM of *nkx2.5:ZsYellow* animals using two-photon excitation time-lapse microscopy. This analysis suggests that ventricular myocardial progenitors are specified in anterior and medial positions relative to pharyngeal progenitors, which reside more laterally and posteriorly (Movies 1 and 2), consistent with the conclusion that progenitor subpopulations are specified in locations approximating their future destinations.

Zebrafish OFT lineages derive from SHF progenitors in PA2

During our prospective lineage tracing of Kaede^{+} cells in PA2, we unexpectedly observed Kaede^{PC+} cells in the OFT of the heart (Fig. 2N,O), a structure known to descend from *nkx2.5*$^{+}$ cells in the zebrafish ALPM (Guner-Ataman et al., 2013) but not by way of PA2. To obtain a qualitative measure of the OFT contributions made by progenitors in PA2, we bilaterally photoconverted them in 28 hpf *Tg(nkx2.5:Kaede)* embryos (Fig. 4A) and analyzed the same animals at 72 hpf for the breadth of Kaede^{PC} labeling in the OFT. The vast majority of cells carrying the native Kaede protein also carried Kaede^{PC} (Fig. 4B-D), indicating that most, if not all, of these OFT cells derive from progenitors in PA2.

It was presumed previously, based on *ltbp3* localization and lineage tracing (Zhou et al., 2011), that SHF OFT progenitors were among the *nkx2.5*$^{+}$ cells that migrate directly to the midline to produce ventricular myocardium (see Introduction). Knowing that the OFT is derived, in large part, from progenitors temporarily sequestered in PA2, we sought to learn whether any OFT cells derive from *nkx2.5*$^{+}$ cells that migrate directly to the midline after specification. To achieve this, we photoconverted Kaede^{+} cells in the cardiac cone (Fig. 4E,F), an intermediate midline structure that becomes the heart tube (Stainier et al., 1993). Consistent with previous studies (Guner-Ataman et al., 2013; Hami et al., 2011; Schoenebeck et al., 2007; Serbedzija et al., 1998), Kaede^{PC} labeling was observed throughout the ventricular myocardium (Fig. 4G,H). However, the OFT was devoid of Kaede^{PC} (Fig. 4G,H), instead carrying the native Kaede protein, demonstrating that the earliest population of *nkx2.5*$^{+}$ cells migrating to the midline does not contribute cells to the OFT. This observation suggests that the OFT labeling we observed previously in *Tg(ltbp3:TagRFP2Acre)* animals resulted from *ltbp3* expression in the OFT proper, or its PA2 progenitors, rather than from the midline population overlapping the cardiac cone at 23 ss (Zhou et al., 2011).

Three OFT lineages derive from SHF progenitors in PA2

To determine which OFT lineages derive from *nkx2.5*$^{+}$ progenitors in PA2, we attempted to colocalize Kaede^{PC+} OFT cells with transgenic reporters in live embryos. However, this approach proved technically impossible because of spectral overlap between the native or photoconverted Kaede protein and available reporters. Moreover, Kaede^{PC} becomes undetectable after fixation, which prevents colocalization by double immunofluorescence staining or

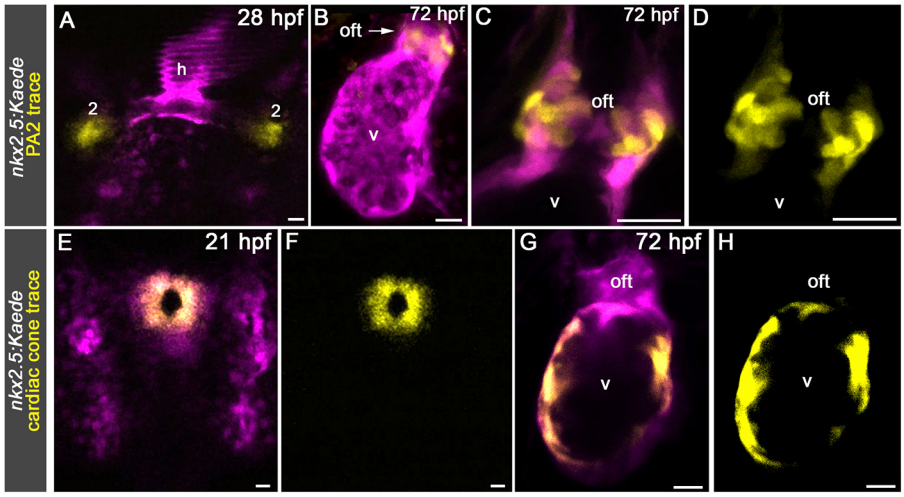

Fig. 4. Unique trajectories of SHF ventricular and OFT progenitors. (A) Confocal *z*-stack of the pharyngeal region in a 28 hpf *Tg(nkx2.5:Kaede)* embryo immediately following bilateral photoconversion of Kaede^{+} cells in pharyngeal arch (PA) 2. A dorsal view is shown. Anterior is upwards. (B) Confocal *z*-stack of the ventricle and OFT in the same embryo at 72 hpf. The arrow highlights OFT cells carrying the photoconverted Kaede protein. All nine animals contained photoconverted cells in the OFT. (C,D) High-magnification confocal *z*-stacks of the OFT in a 72 hpf *Tg(nkx2.5:Kaede)* animal in which Kaede^{+} cells in PA2 were photoconverted bilaterally at 28 hpf. (E,F) Confocal *z*-stacks of a 21 hpf *Tg(nkx2.5:Kaede)* embryo immediately following photoconversion of Kaede^{+} cells in the cardiac cone. A dorsal view is shown. Anterior is upwards. (G,H) Confocal *z*-stack of the ventricle and OFT in the same embryo at 72 hpf. All 12 animals contained photoconverted cells in the ventricle but not in the OFT. All animals in A-H were imaged in the green (pseudocolored magenta) and red (pseudocolored yellow) channels. Merged (A-C,E,G) and single-channel (D,F,H) images are shown. Cardiac structures: h, heart; oft, outflow tract; v, ventricle. Scale bars: 25 µm.

Development (2017) 144, 4616-4624 doi:10.1242/dev.153411

in situ hybridization. Nonetheless, based on the broad localization of lineage-traced cells in the OFT (Fig. 4C,D), we speculate that all three OFT lineages are labeled. Specifically, Kaede^{PC+} cells were observed at the base of the OFT (Fig. 5C-E,I-K,O-Q) where cardiomyocytes are localized [Fig. 5A-B′; (Grimes et al., 2006)]. They also resided within the Eln2^{+} smooth muscle wall of the OFT (Fig. 5C-E,F-H,L-N, and O-Q), which extends from the myocardial base to the ventral aorta (Fig. 5A-B′) (Grimes et al., 2006; Miao et al., 2007). Last, Kaede^{PC+} cells were observed internally (Fig. 5I-Q), where OFT endocardium forms the lumen (Fig. 5A-B′). Taken together, our data identify PA2 as a novel source of three OFT lineages during zebrafish embryogenesis. A small number of neural crest-derived cells have been reported to colonize the OFT but subsequent to the stages we analyzed (Cavanaugh et al., 2015).

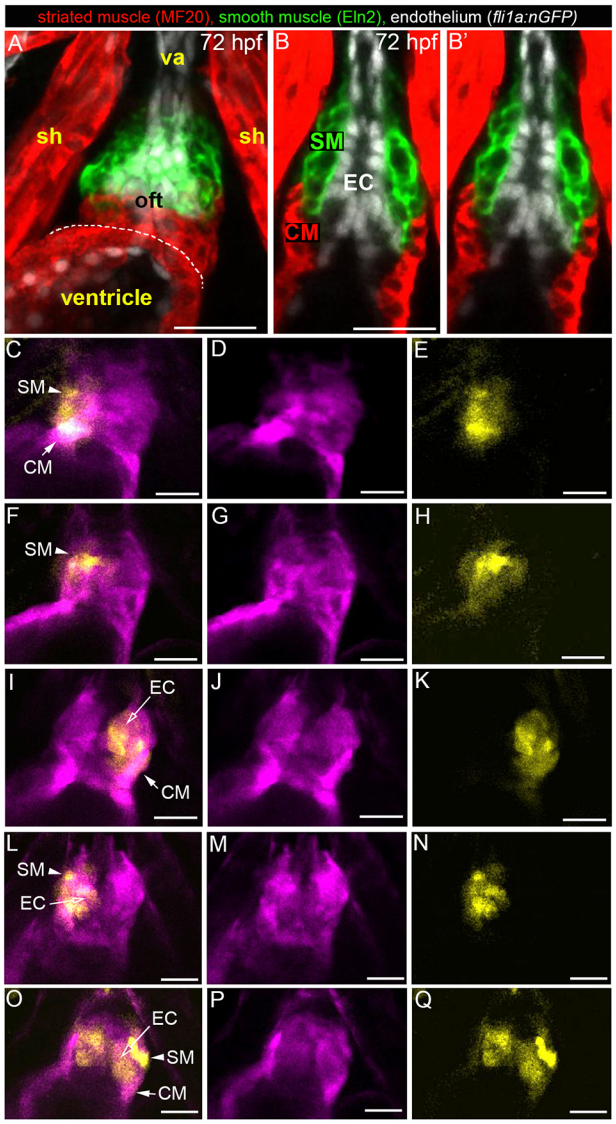

Fig. 5. PA2 progenitors give rise to three OFT lineages. (A,B) Confocal images of the OFT in a 72 hpf *Tg(fli1a:nGFP)* embryo triple immunostained to detect OFT myocardium (MF20 antibody, red), smooth muscle (α-Eln2 antibody, green) and endothelium (α-GFP antibody, white). A *z*-stack (A) and single planes (B,B′) are shown. B′ is a duplicate of B without the labels and provides an unimpeded view of the physical relationships between OFT lineages. OFT endocardium is surrounded by two collars of muscle, a myocardial collar abutting the ventricle and an adjacent smooth muscle collar that extends to the ventral aorta. (C-Q) Single planes from confocal *z*-stacks of OFTs in 72 hpf live *Tg(nkx2.5:Kaede)* embryos in which right-sided (C-H,L-N), left-sided (I-K) or bilateral (O-Q) photoconversion of Kaede^{+} cells in PA2 was performed at 28 hpf. OFT cells carrying the native (pseudocolored magenta) and photoconverted (pseudocolored yellow) Kaede protein are shown. Merged (C,F,I,L,O) and single-channel (D,E,G,H,J,K,M,N,P,Q) images are shown. The lineage identities of the labeled cells (arrows) were inferred based on location. Ventral views, anterior up. sh, sternohyoideus muscle; va, ventral aorta; oft, outflow tract; SM, smooth muscle; EC, endocardium; CM, cardiomyocytes. Scale bars: 25 µm.

SHF ventricular progenitors are uniquely sensitive to perturbations in Fgf8a signaling

Finally, to determine if the observed partitioning of SHF ventricular and OFT progenitors confers each population with unique genetic sensitivities, we analyzed *acerebellar* (*ace*) mutant embryos, which harbor a mutation in *fgf8a* (Reifers et al., 1998), for defects in HM and OFT morphogenesis. Previous studies have demonstrated that inactivation of *fgf8a*, or chemical inhibition of FGF receptor activity, results in a deficiency of SHF progenitors at the arterial pole (Lazic and Scott, 2011; Zeng and Yelon, 2014) and reductions in SHF-derived ventricular cardiomyocytes (de Pater et al., 2009; Lazic and Scott, 2011). We sought to determine if *ace* embryos also harbor defects in OFT and HM morphogenesis. First, we analyzed 28 hpf *ace* animals carrying the *nkx2.5:ZsYellow* transgene, which labels extra-cardiac SHF progenitors at the arterial pole of the linear heart tube (Zhou et al., 2011) and precursors for HM, HA endothelium and OFT lineages in PA2 (Fig. 2M-P, Fig. 4A-D). Consistent with previous studies (Reifers et al., 1998; Zeng and Yelon, 2014; Zhou et al., 2011), extra-cardiac SHF ventricular progenitors were reduced or absent (Fig. 6A,B). However, the ZsYellow^{+} progenitor population in PA2 was grossly unaffected (Fig. 6A,B). Next, we analyzed 72 hpf *ace* animals double immunostained to visualize ventricular, OFT and head muscle (MF20 antibody) as well as Eln2^{+} OFT smooth muscle cells. Consistent with previous reports, the ventricles in *ace* mutants were smaller than those in siblings (Fig. 6C,D) owing to a reported combination of ventricular progenitor specification and cardiomyocyte accretion defects (de Pater et al., 2009; Marques et al., 2008). By contrast, the OFTs in *ace* animals appeared grossly unperturbed (Fig. 6C,D), containing normal numbers of Eln2^{+} smooth muscle cells (Fig. 6E-G), indicating that the mutation preferentially impacts ventricular morphogenesis. In greater than half of the mutant animals (14/25), the PA1 and PA2 HMs were indistinguishable from siblings (Fig. 6H-K). In the rest, HMs were largely present but partially mispatterned (Fig. S3A,B), perhaps attributable to pharyngeal laterality defects, which have been reported to affect a similar fraction of *ace* animals (Albertson and Yelick, 2005). Taken together, these data demonstrate that the physical partitioning of *nkx2.5*$^{+}$ SHF ventricular and OFT progenitors, which occurs soon after their specification, confers each population with unique genetic requirements during their maturation.

DISCUSSION

Our study highlights previously unappreciated aspects of SHF, OFT and HM development in zebrafish that appear to be consistent with findings in higher vertebrates. The *nkx2.5* lineage in mouse embryos gives rise to head muscles derived from PA1 and PA2 (Harel et al., 2009). Furthermore, dye-tracing experiments in avian and rodent embryos suggest that progenitor cells in the anterior PAs contribute myocardium to the embryonic outflow tract (Kelly et al., 2001; Nathan et al., 2008; Tirosh-Finkel et al., 2006). In addition, retrospective clonal analysis in the mouse uncovered a clonal

Development (2017) 144, 4616-4624 doi:10.1242/dev.153411

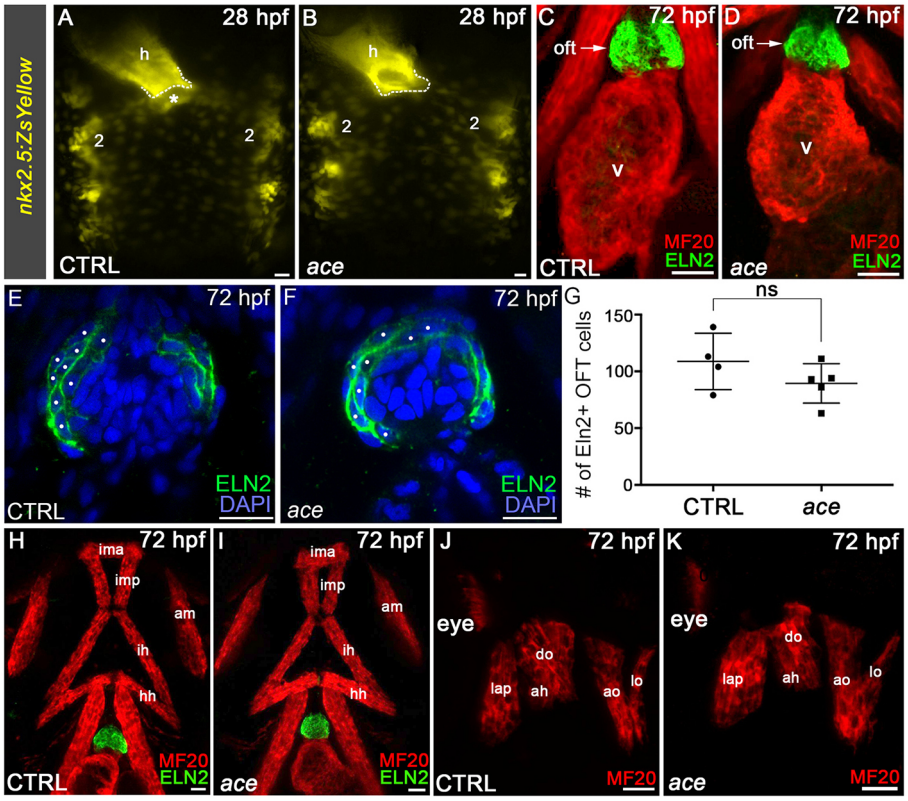

Fig. 6. SHF ventricular and OFT progenitors are uniquely sensitive to perturbations in Fgf8a signaling. (A,B) Compound microscopic images of live 28 hpf control (CTRL) sibling (A) or *ace* (B, *n*=33) embryos carrying the *nkx2.5:ZsYellow* transgene. Dorsal views are shown. Anterior is upwards. The dotted lines demarcate the arterial pole of the heart tube. The asterisk highlights extra-cardiac ZsYellow^{+} anterior SHF progenitors absent in *ace* mutants. All 74 control and all *ace* animals displayed the ZsYellow distributions shown. (C,D) Confocal *z*-stacks of the ventricle and OFT in 72 hpf CTRL and *ace* animals double immunostained to detect striated muscle (MF20 antibody) and Eln2^{+} smooth muscle OFT cells imaged in the red and green channels, respectively. All 76 control and all 25 *ace* animals contained Eln2^{+} OFTs. Ventral views. Anterior is upwards. (E,F) Confocal *z*-stacks of the OFTs in 72 hpf CTRL and *ace* mutant embryos immunostained to visualize Eln2 (green) and counterstained with DAPI (blue) to detect nuclei. White dots highlight nuclei in cells surrounded by Eln2. (G) Dot plot showing the quantification of Eln2^{+} OFT cells in 72 hpf control and *ace* mutant embryos. An unpaired *t*-test was used to evaluate statistical significance. ns, not significant. (H-K) Confocal *z*-stacks of pharyngeal regions in 72 hpf control and *ace* animals double immunostained to detect striated muscle (MF20 antibody) and Eln2^{+} smooth muscle OFT cells imaged in the red and green channels, respectively. All 76 CTRL and 14/25 *ace* animals contained the head muscles in the pattern shown. Ventral (H,I) and lateral (J,K) views are shown. Anterior is upwards (H,I) or leftwards (J,K). Number two labels pharyngeal arch 2. h, heart. Ventral pharyngeal arch (PA) 1 (mandibular) muscle: ima, intermandibular anterior. Middle PA1 muscles: imp, intermandibular posterior; am, adductor mandibulae. Dorsal PA1 muscles: lap, levator arcus palatine; do, dilator operculi. Ventral PA2 (hyoid) muscle: ih, interhyal. Middle PA2 muscle: hh, hyohyal. Dorsal PA2 muscles: ah, adductor hyomandibulae; ao, adductor operculi; lo, levator operculi. Cardiac structures: oft, outflow tract; v, ventricle. Scale bars: 25 µm.

relationship between OFT cardiomyocytes and head muscles that derive from PA2 (Lescroart et al., 2010), suggesting that OFT progenitors are also temporarily sequestered in PA2 in mammals. Despite these precedents in higher vertebrates, our study is the first to achieve spatiotemporally localized prospective lineage tracing of a genetically labeled HM and OFT progenitor population in PA2. Although our studies cannot reveal that, as in higher vertebrates (Lescroart et al., 2010), HM and OFT progenitors share a common progenitor, it is tempting to speculate that one exists based on the similarities in specification and shared trajectories to PA2. Taken together, our findings uncover additional similarities between SHF, OFT and HM development in zebrafish and higher vertebrates that validate the use of zebrafish in deciphering SHF biology in the context of human congenital heart disease models.

MATERIALS AND METHODS

Zebrafish husbandry and strains

Zebrafish adults and embryos were maintained as previously described (Westerfield, 2007), which was approved by the Massachusetts General Hospital Institutional Animal Care and Use Committee. The strains used in experimental studies included: wild-type TuAB; *ace* mutants (Reifers et al., 1998); *Tg(ubi:loxP-EGFP-loxP-mCherry)*^{cz1701} [*Tg(ubi:Switch)*] (Mosimann et al., 2015); *Tg(fli1a:EGFP)*^{y1} (Roman et al., 2002); *Tg(fli1a:nEGFP)*^{y7} (Roman et al., 2002); *Tg(-36nkx2.5:ZsYellow)*^{fb7} (Zhou et al., 2011); *TgBAC(-36nkx2.5:ERCreERt2)*^{fb8} (Guner-Ataman et al., 2013); *TgBAC(-36nkx2.5:Kaede)*^{fb9} (Guner-Ataman et al., 2013); and *Tg(-4.9sox10:EGFP)*^{ba2} (Carney et al., 2006). Unless specified, live embryos were kept at 28.5°C and anesthetized in standard embryo media containing 0.4% tricaine (ethyl 3-aminobenzoate methanesulfonate, MS222; Sigma).

Genetic lineage tracing

Adult zebrafish carrying the *nkx2.5:ERCreER*^{t2} driver transgene were crossed with *Tg(ubi:loxP-EGFP-loxP-mCherry)*^{cz1701} animals. The resulting progeny were collected according to standard zebrafish protocols (Westerfield, 2007) and raised to tailbud stage. For experimental treatments, tailbud stage embryos were incubated in 10 µM 4-hydroxytamoxifen (4-OHT) in embryo medium (E3) for a total of 5-7 h. For mock treatments, 4-OHT was replaced with an equivalent volume of 100% ethanol, which is the standard solvent for the 10 mM 4-OHT stock solution. After 5-7 h, the 12-16 ss embryos were washed with 50 ml E3 three times and raised to 72 hpf for subsequent antibody staining and imaging. The presence of the *ubi:loxP-EGFP-loxP-mCherry* allele was identified by screening for ubiquitous EGFP activity. The presence of the *nkx2.5:ERCreER*^{t2} allele was inferred from evidence of Cre activity through mCherry expression.

Development (2017) 144, 4616-4624 doi:10.1242/dev.153411

Whole-mount *in situ* hybridization and immunohistochemistry

Single whole-mount *in situ* hybridizations were performed in glass vials as previously described (Thisse and Thisse, 2008). Digoxygenin-labeled antisense RNA probes to *nkx2.5* (Reiter et al., 1999) and *ZsYellow* were synthesized using a DIG RNA Labeling Kit (SP6/T7; Roche). To generate the *ZsYellow* riboprobe, a plasmid containing the full-length *ZsYellow* sequence (pCRBIITOPO ZsYellow *Bam*HI/*Cla*I rev) was digested with *Not*I and transcribed with SP6 polymerase. A blue (NBT/BCIP) chromogenic substrate was used (Roche). For immunohistochemistry, manipulations were performed at room temperature unless otherwise stated. Embryos were fixed overnight in 4% PFA at 4°C and then washed at room temperature with phosphate-buffered saline (pH 7.4), 0.1% Tween-20 (PBST) four times for 10 min. Embryos were incubated in a bleach solution (0.5% KOH/3% H_2O_2/0.1% Tween-20) in the dark until pigment was removed and washed four times for 10 min with PBST. Permeabilization was achieved by incubating embryos in PBS/0.5% Triton X-100 (PBSTx) for 2 h followed by incubation in block solution (5% bovine serum albumin/5% goat serum in PBST) for 2 h. Embryos were incubated with primary antibodies diluted in block solution overnight at 4°C. Embryos were washed six times for 20 min in PBST and incubated with secondary antibodies diluted in block (1:500) overnight at 4°C. Secondary antibodies were removed by washing with PBST six times for 20 min prior to imaging or storage at 4°C in PBST. Primary antibodies specific for GFP (1:50, A11122, Invitrogen), MF20 (1:50, University of Iowa), Eln2 (1:1000) (Miao et al., 2007), mCherry (1:50, ab167453, Abcam) and ZsYellow (1:50, 632475, Clontech).

Identification of *ace* mutants

Mutant *ace* embryos were identified by PCR amplification and sequencing of the mutation-containing region of the genome (Reifers et al., 1998) using the following primers: 5′-ACG GAC ACA TTT GGG AGT CG-3′ and 5′-GGT GGG ATT CTT CTC ATG CAT TC-3′. The latter primer was used to sequence the purified PCR product.

Kaede photoconversion

Live *TgBAC(-36nkx2.5:Kaede)*^{fb9} embryos were positioned and embedded in 0.9% low melting point agarose in 35 mm glass-bottom Petri dishes, covered with embryo media and 0.4% Tricaine, and photoconverted with either a Zeiss LSM5 Pascal Laser-Scanning Microscope or a Nikon Eclipse Ti Confocal Microscope, as previously described (Guner-Ataman et al., 2013). Animals were pre-screened for signs of spontaneous photoconversion, which was never observed. Photoconversion was then achieved by manually setting the desired exposure area on the animal and performing a brief *z*-stack under UV light. Animals with imprecise photoconversion were excluded from further analysis. Post-photoconversion images were collected with the 488 and 546 lasers. Embryos were carefully extracted from the agarose gel and raised individually until subsequent analysis. Extreme care was taken to minimize light exposure for the duration of the experiment.

Microscopy and imaging

Embryos processed for *in situ* hybridization were mounted on glass slides in 100% glycerol (Thisse and Thisse, 2008). For fluorescent imaging, embryos were embedded in 0.9% low melting point agarose (NuSieve GTG Agarose, Lonza) in 35 mm glass-bottom Petri dishes (MatTek Corporation). Fixed embryos were covered with PBST. Live embryos were covered with embryo media containing 0.4% tricaine. To arrest cardiac activity, 80 µM 2,3-butanedione monoxime (Sigma Aldrich) was also added. Live or processed embryos were imaged on a Nikon 80i compound microscope. Images of embryos processed by *in situ* hybridization were captured using a mounted Excelis AU600HDS HD Camera (Accu-Scope) and the resulting images were focus-stacked with Zerene Stacker Software (Build T201412212230). Confocal microscopy was performed using either a Zeiss LSM5 Pascal Laser-Scanning Microscope or a Nikon A1SiR Confocal Microscope. Time-lapse imaging was performed using a 514 nm argon laser and 25× objective on a Nikon A1R Multiphoton Confocal Microscope. Embryos were embedded in low-melt agarose to prevent movement. *Z*-stack images and time-lapse movies were viewed and analyzed with ImageJ (Schneider et al., 2012) and Fiji (Schindelin et al., 2012) software.

Quantification of Eln2$^+$ OFT smooth muscle cells

Eln2$^+$ OFT smooth muscle cell nuclei were quantified in Fiji by generating RGB images of confocal *z*-stacks in which the DAPI signals were pseudocolored blue and the Eln2 signals were pseudocolored green. Nuclei in cells surrounded by Eln2 were identified while scrolling through the *z*-stacks and marked with dots in the red channel using the paintbrush tool to avoid double counting. After splitting the three channels, the 3D object counter tool was used to quantify the number of dots present in the red channel, which corresponded to the total number of Eln2$^+$ cell nuclei in the OFT.

Acknowledgements

We thank J. M. González-Rosa from the Burns laboratory for useful discussions and advice on immunohistochemistry, confocal imaging and *ace* genotyping; J. Galloway (Massachusetts General Hospital) for providing expertise on muscle populations and early muscle development; and T. Schilling (University of California, Irvine) for providing expertise on pharyngeal segmentation and muscles.

Competing interests

The authors declare no competing or financial interests.

Author contributions

Conceptualization: C.G.B., C.E.B., N.P.-L.; Methodology: C.G.B., C.E.B., N.P.-L., N.N.; Validation: C.G.B., C.E.B., N.P.-L., N.N.; Investigation: N.P.-L., N.N., S.J., M.A., B.G.-A., S.S.; Resources: C.G.B., C.E.B.; Writing - original draft: C.G.B., C.E.B.; Writing - review & editing: C.G.B., C.E.B., N.P.-L., N.N.; Visualization: C.G.B., C.E.B., N.P.-L., N.N.; Supervision: C.G.B., C.E.B.; Project administration: C.G.B., C.E.B.; Funding acquisition: C.G.B., C.E.B.

Funding

This work was supported by the National Institutes of Health (R01HL096816 to C.G.B., and R01HL111179 and R35HL135831 to C.E.B.). C.G.B. received an award from the Executive Committee on Research at Massachusetts General Hospital to support this work. C.E.B. is a d'Arbelhoff Massachusetts General Hospital Research Scholar. N.P.-L. was supported by the Harvard Stem Cell Institute Training Grant (5HL087735), by a National Institutes of Health National Research Service Award (F32HL112579) and by a Massachusetts General Hospital Tosteson Award. N.N. was supported by a National Institutes of Health Training Grant (T32HL007208). M.A. received support from a Servier Institute International Mobility Help Grant and a Victor A. McKusick Fellowship from the Marfan Foundation (2016D001458). B.G.-A. was supported by a Scientist Development Grant (14SDG19020018) from the American Heart Association. Deposited in PMC for release after 12 months.

Supplementary information

Supplementary information available online at
http://dev.biologists.org/lookup/doi/10.1242/dev.153411.supplemental

References

Abu-Issa, R. and Kirby, M. L. (2007). Heart field: from mesoderm to heart tube. *Annu. Rev. Cell Dev. Biol.* **23**, 45-68.

Albertson, R. C. and Yelick, P. C. (2005). Roles for fgf8 signaling in left-right patterning of the visceral organs and craniofacial skeleton. *Dev. Biol.* **283**, 310-321.

Bajolle, F., Zaffran, S., Kelly, R. G., Hadchouel, J., Bonnet, D., Brown, N. A. and Buckingham, M. E. (2006). Rotation of the myocardial wall of the outflow tract is implicated in the normal positioning of the great arteries. *Circ. Res.* **98**, 421-428.

Benjamin, E. J., Blaha, M. J., Chiuve, S. E., Cushman, M., Das, S. R., Deo, R., de Ferranti, S. D., Floyd, J., Fornage, M., Gillespie, C. et al. (2017). Heart disease and stroke statistics-2017 update: a report from the American Heart Association. *Circulation* **135**, e146-e603.

Carney, T. J., Dutton, K. A., Greenhill, E., Delfino-Machín, M., Dufourcq, P., Blader, P. and Kelsh, R. N. (2006). A direct role for Sox10 in specification of neural crest-derived sensory neurons. *Development* **133**, 4619-4630.

Cavanaugh, A. M., Huang, J. and Chen, J.-N. (2015). Two developmentally distinct populations of neural crest cells contribute to the zebrafish heart. *Dev. Biol.* **404**, 103-112.

de Pater, E., Clijsters, L., Marques, S. R., Lin, Y.-F., Garavito-Aguilar, Z. V., Yelon, D. and Bakkers, J. (2009). Distinct phases of cardiomyocyte differentiation regulate growth of the zebrafish heart. *Development* **136**, 1633-1641.

Grimes, A. C., Stadt, H. A., Shepherd, I. T. and Kirby, M. L. (2006). Solving an enigma: arterial pole development in the zebrafish heart. *Dev. Biol.* **290**, 265-276.
Grimes, A. C., Durán, A. C., Sans-Coma, V., Hami, D., Santoro, M. M. and Torres, M. (2010). Phylogeny informs ontogeny: a proposed common theme in the arterial pole of the vertebrate heart. *Evol. Dev.* **12**, 552-567.
Guner-Ataman, B., Paffett-Lugassy, N., Adams, M. S., Nevis, K. R., Jahangiri, L., Obregon, P., Kikuchi, K., Poss, K. D., Burns, C. E. and Burns, C. G. (2013). Zebrafish second heart field development relies on progenitor specification in anterior lateral plate mesoderm and nkx2.5 function. *Development* **140**, 1353-1363.
Hami, D., Grimes, A. C., Tsai, H.-J. and Kirby, M. L. (2011). Zebrafish cardiac development requires a conserved secondary heart field. *Development* **138**, 2389-2398.
Harel, I., Nathan, E., Tirosh-Finkel, L., Zigdon, H., Guimarães-Camboa, N., Evans, S. M. and Tzahor, E. (2009). Distinct origins and genetic programs of head muscle satellite cells. *Dev. Cell* **16**, 822-832.
Kelly, R. G., Brown, N. A. and Buckingham, M. E. (2001). The arterial pole of the mouse heart forms from Fgf10-expressing cells in pharyngeal mesoderm. *Dev. Cell* **1**, 435-440.
Kirby, M. L. (2007). *Cardiac Development*. Oxford, UK: Oxford University Press.
Lawson, N. D. and Weinstein, B. M. (2002). In vivo imaging of embryonic vascular development using transgenic zebrafish. *Dev. Biol.* **248**, 307-318.
Lazic, S. and Scott, I. C. (2011). Mef2cb regulates late myocardial cell addition from a second heart field-like population of progenitors in zebrafish. *Dev. Biol.* **354**, 123-133.
Lee, K.-H., Xu, Q. and Breitbart, R. E. (1996). A new tinman-related gene, nkx2.7, anticipates the expression of nkx2.5 and nkx2.3 in zebrafish heart and pharyngeal endoderm. *Dev. Biol.* **180**, 722-731.
Lescroart, F., Kelly, R. G., Le Garrec, J.-F., Nicolas, J.-F., Meilhac, S. M. and Buckingham, M. (2010). Clonal analysis reveals common lineage relationships between head muscles and second heart field derivatives in the mouse embryo. *Development* **137**, 3269-3279.
Marques, S. R., Lee, Y., Poss, K. D. and Yelon, D. (2008). Reiterative roles for FGF signaling in the establishment of size and proportion of the zebrafish heart. *Dev. Biol.* **321**, 397-406.
Miao, M., Bruce, A. E. E., Bhanji, T., Davis, E. C. and Keeley, F. W. (2007). Differential expression of two tropoelastin genes in zebrafish. *Matrix Biol.* **26**, 115-124.
Mosimann, C., Kaufman, C. K., Li, P., Pugach, E. K., Tamplin, O. J. and Zon, L. I. (2011). Ubiquitous transgene expression and Cre-based recombination driven by the ubiquitin promoter in zebrafish. *Development* **138**, 169-177.
Mosimann, C., Panáková, D., Werdich, A. A., Musso, G., Burger, A., Lawson, K. L., Carr, L. A., Nevis, K. R., Sabeh, M. K., Zhou, Y. et al. (2015). Chamber identity programs drive early functional partitioning of the heart. *Nat. Commun.* **6**, 8146.
Nagelberg, D., Wang, J., Su, R., Torres-Vázquez, J., Targoff, K. L., Poss, K. D. and Knaut, H. (2015). Origin, specification, and plasticity of the great vessels of the heart. *Curr. Biol.* **25**, 2099-2110.
Nathan, E., Monovich, A., Tirosh-Finkel, L., Harrelson, Z., Rousso, T., Rinon, A., Harel, I., Evans, S. M. and Tzahor, E. (2008). The contribution of Islet1-expressing splanchnic mesoderm cells to distinct branchiomeric muscles reveals significant heterogeneity in head muscle development. *Development* **135**, 647-657.
Nevis, K., Obregon, P., Walsh, C., Guner-Ataman, B., Burns, C. G. and Burns, C. E. (2013). Tbx1 is required for second heart field proliferation in zebrafish. *Dev. Dyn.* **242**, 550-559.
Paffett-Lugassy, N., Singh, R., Nevis, K. R., Guner-Ataman, B., O'Loughlin, E., Jahangiri, L., Harvey, R. P., Burns, C. G. and Burns, C. E. (2013). Heart field origin of great vessel precursors relies on nkx2.5-mediated vasculogenesis. *Nat. Cell Biol.* **15**, 1362-1369.
Reifers, F., Böhli, H., Walsh, E. C., Crossley, P. H., Stainier, D. Y. and Brand, M. (1998). Fgf8 is mutated in zebrafish acerebellar (ace) mutants and is required for maintenance of midbrain-hindbrain boundary development and somitogenesis. *Development* **125**, 2381-2395.
Reiter, J. F., Alexander, J., Rodaway, A., Yelon, D., Patient, R., Holder, N. and Stainier, D. Y. R. (1999). Gata5 is required for the development of the heart and endoderm in zebrafish. *Genes Dev.* **13**, 2983-2995.
Roman, B. L., Pham, V. N., Lawson, N. D., Kulik, M., Childs, S., Lekven, A. C., Garrity, D. M., Moon, R. T., Fishman, M. C., Lechleider, R. J. et al. (2002). Disruption of acvrl1 increases endothelial cell number in zebrafish cranial vessels. *Development* **129**, 3009-3019.
Schilling, T. F. and Kimmel, C. B. (1994). Segment and cell type lineage restrictions during pharyngeal arch development in the zebrafish embryo. *Development* **120**, 483-494.
Schilling, T. F. and Kimmel, C. B. (1997). Musculoskeletal patterning in the pharyngeal segments of the zebrafish embryo. *Development* **124**, 2945-2960.
Schindelin, J., Arganda-Carreras, I., Frise, E., Kaynig, V., Longair, M., Pietzsch, T., Preibisch, S., Rueden, C., Saalfeld, S., Schmid, B. et al. (2012). Fiji: an open-source platform for biological-image analysis. *Nat. Methods* **9**, 676-682.
Schneider, C. A., Rasband, W. S. and Eliceiri, K. W. (2012). NIH Image to ImageJ: 25 years of image analysis. *Nat. Methods* **9**, 671-675.
Schoenebeck, J. J., Keegan, B. R. and Yelon, D. (2007). Vessel and blood specification override cardiac potential in anterior mesoderm. *Dev. Cell* **13**, 254-267.
Serbedzija, G. N., Chen, J. N. and Fishman, M. C. (1998). Regulation in the heart field of zebrafish. *Development* **125**, 1095-1101.
Stainier, D. Y., Lee, R. K. and Fishman, M. C. (1993). Cardiovascular development in the zebrafish. I. Myocardial fate map and heart tube formation. *Development* **119**, 31-40.
Stanley, E. G., Biben, C., Elefanty, A., Barnett, L., Koentgen, F., Robb, L. and Harvey, R. P. (2002). Efficient Cre-mediated deletion in cardiac progenitor cells conferred by a 3'UTR-ires-Cre allele of the homeobox gene Nkx2-5. *Int. J. Dev. Biol.* **46**, 431-439.
Thisse, C. and Thisse, B. (2008). High-resolution in situ hybridization to whole-mount zebrafish embryos. *Nat. Protoc.* **3**, 59-69.
Tirosh-Finkel, L., Elhanany, H., Rinon, A. and Tzahor, E. (2006). Mesoderm progenitor cells of common origin contribute to the head musculature and the cardiac outflow tract. *Development* **133**, 1943-1953.
Vincent, S. D. and Buckingham, M. E. (2010). How to make a heart: the origin and regulation of cardiac progenitor cells. *Curr. Top. Dev. Biol.* **90**, 1-41.
Waldo, K. L., Hutson, M. R., Ward, C. C., Zdanowicz, M., Stadt, H. A., Kumiski, D., Abu-Issa, R. and Kirby, M. L. (2005). Secondary heart field contributes myocardium and smooth muscle to the arterial pole of the developing heart. *Dev. Biol.* **281**, 78-90.
Watanabe, M., Choudhry, A., Berlan, M., Singal, A., Siwik, E., Mohr, S. and Fisher, S. A. (1998). Developmental remodeling and shortening of the cardiac outflow tract involves myocyte programmed cell death. *Development* **125**, 3809-3820.
Westerfield, M. (2007). *The Zebrafish Book. A Guide for the Laboratory use of Zebrafish (Danio rerio)*, 4th edn. Eugene, OR: University of Oregon Press.
Zaffran, S. and Kelly, R. G. (2012). New developments in the second heart field. *Differentiation* **84**, 17-24.
Zeng, X.-X. I. and Yelon, D. (2014). Cadm4 restricts the production of cardiac outflow tract progenitor cells. *Cell Rep.* **7**, 951-960.
Zhang, L., Nomura-Kitabayashi, A., Sultana, N., Cai, W., Cai, X., Moon, A. M. and Cai, C.-L. (2014). Mesodermal Nkx2.5 is necessary and sufficient for early second heart field development. *Dev. Biol.* **390**, 68-79.
Zhou, Y., Cashman, T. J., Nevis, K. R., Obregon, P., Carney, S. A., Liu, Y., Gu, A., Mosimann, C., Sondalle, S., Peterson, R. E. et al. (2011). Latent TGF-β binding protein 3 identifies a second heart field in zebrafish. *Nature* **474**, 645-648.